J Mater Sci (2010) 45:443–447
DOI 10.1007/s10853-009-3960-3

A first principles investigation of isotactic polypropylene

M. E. Stournara · R. Ramprasad

Received: 27 August 2009 / Accepted: 5 October 2009 / Published online: 20 October 2009

Abstract Bulk isotactic polypropylene in the α form was studied using density functional theory-based computations. The computed physical structure of this system is in excellent agreement with available experimental data. The electronic band structure, ionization potential, and electron affinity were also determined. The impact of various types of chemical imperfections (including double bond, hydroxyl, and carbonyl defects) on the electronic structure of bulk isotactic polypropylene was considered. The carbonyl defect was found to cause the most significant impact, resulting in the deepest electron and hole traps.

Introduction

Polypropylene, being one of the fastest growing engineering plastics, has wide industrial and everyday applications due to attractive properties such as low density, high melting point, high tensile strength, and a high resistance to chemical attack [1]. A major application area where (biaxially oriented) polypropylene has already found a niche is in electrical cable and capacitor dielectric systems [2–6]. Demands for further improvements in the electrical performance of the polypropylene dielectric continues, in terms of higher dielectric breakdown strength and lower high-field electrical conduction. Such a need provides the motivation for the present ab initio study of the electronic properties of defect-free and defective polypropylene.

M. E. Stournara · R. Ramprasad (✉)
Department of Chemical, Materials and Biomolecular Engineering, Institute of Materials Science, University of Connecticut, 97 North Eagleville Road, Storrs, CT 06269, USA
e-mail: rampi@ims.uconn.edu

Crystalline polypropylene can occur in two forms: isotactic, in which the methyl group of the –[$CH_2CH(CH_3)$]– mer units are along the same side of the polymer backbone, and syndiotactic, in which the methyl units are on opposite sides. An atactic variety, in which adjacent methyl units are randomly arranged on either sides of the polymer backbone, is also possible, but this form is not crystalline as a periodically repeating unit cell cannot be formally defined. This study focuses primarily on isotactic polypropylene (iPP), which occurs in three different bulk polymorphs depending on how the isotactic chains are packed: monoclinic α, hexagonal β, and triclinic γ. Among these three polymorphs, α-isotactic polypropylene (α-iPP) is the most stable and commonly observed. While extensive experimental work has been aimed at the physical characterization of the different bulk phases [7–17], only isolated chains of iPP have been studied before computationally [18–20].

In this paper, we present ab initio density functional theory (DFT) based calculations aimed at a basic understanding of the physical and electronic structure of α-iPP. We begin by providing details concerning our DFT calculations in "Methodology" section. Results related to the physical structure of a single chain of iPP and bulk α-iPP are provided in "Physical structure of isotactic polypropylene" section, followed by a discussion of their band structure in "Electronic structure of defect-free iPP." We then report on the computation of the ionization potential and electron affinity using slab supercells in "Ionization potential and electron affinity" section. In "Chemical imperfections and electronic structure" section, we consider chemical imperfections, including hydroxyl, carbonyl, and double bond defects, in bulk α-iPP, and explore the impact of these defects on the electronic structure. We find that the carbonyl defect results in deep electron and

hole trap states. Finally, we summarize our findings "Summary" section.

Methodology

Our DFT calculations were performed using the Vienna ab initio simulation package (VASP) [21] with the PW91 generalized gradient approximation [22], projector-augumented wave (PAW) pseudopotentials [23, 24] and a cutoff energy of 400 eV for the plane wave expansion of the wavefunctions. Monkhorst-Pack k-point sampling meshes of $(1 \times 1 \times 4)$ and $(1 \times 2 \times 2)$ were used to treat the isolated iPP chain and the bulk α-iPP systems, respectively. Bond lengths, bond angles, and unit cell vectors were all optimized such that the energy changes in successive geometry optimization iterations were smaller than 10^{-4} eV.

Results and discussion

Physical structure of isotactic polypropylene

The α-iPP monoclinic unit cell consists of four (3/1) helical chains (see Fig. 1). Each (3/1) helical chain is composed of three –[$CH_2CH(CH_3)$]– units forming the "pitch" of the helix. Before discussing crystalline α-iPP, we first consider an isolated (3/1) helical chain. For comparison, we also consider a non-helical isotactic zig-zag chain in which a single –[$CH_2CH(CH_3)$]– mer forms a periodic unit with all the methyl groups aligned. Both isolated chains were separated from their adjacent periodic images along directions perpendicular to the chain axis by about 10 Å to minimize spurious interchain interactions. The structural parameters of the chains were optimized with respect to the atomic positions as well as the periodic distance along the chain axis. We found that the energy of the helical conformation is 1.038 eV per –[$CH_2CH(CH_3)$]– unit lower than the straight zig-zag form, denoting that the ionic interaction between adjacent methyl groups does not favor the formation of a straight zig-zag chain and is, thus, responsible for the formation of a (3/1) helix. Table 1 lists the optimized structural details of the (3/1) helical chain as determined here, and compares these with available prior computational determinations [18].

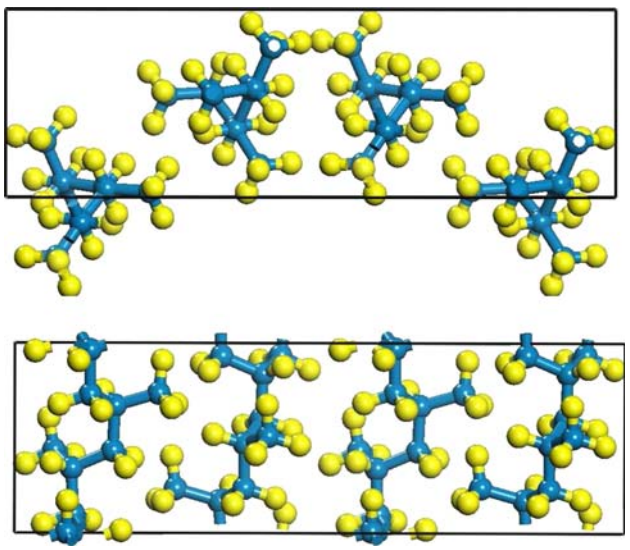

Fig. 1 Atomic model of monoclinic α-iPP, projected in planes normal to the *c* (top) and *a* (bottom) axes of the monoclinic unit cell. C and H atoms are shown as dark (blue) and light (yellow) spheres, respectively. (Color figure online)

Next, we consider the α-iPP crystal (space group *Cc*), whose structure was first proposed by Natta and Corradini [7] (see Fig. 1). As mentioned above, each unit cell contains four separate (3/1) helical chains, with each chain composed of three –$CH_2CH(CH_3)$– units (totalling 108 atoms per unit cell). Two of the chains are right-handed helices whereas the other two are left-handed helices, with the two pairs related to each other by mirror and translational symmetry. Table 1 also shows the final optimized geometric details of α-iPP, along with a comparison with available experimental data [7, 17]. As can be seen, the agreement with experiment is quite reasonable.

Electronic structure of defect-free iPP

For the case of the (3/1) helical chain, the band structure was computed in the $(0 - \frac{\pi}{c})$ region of reciprocal space, with c = 6.49 Å being the periodic length along the chain axis, whereas for bulk α-iPP it was calculated along the symmetric lines in the Brillouin zone corresponding to the monoclinic unit cell [25]. These results together with the corresponding density of states (DOS) plots are presented in Figs. 2 and 3, for the chain and bulk cases, respectively. In both cases the band gap is direct, with values of 5.8 and 6.3 eV for the isolated helical chain and bulk α-iPP, respectively. The chain band gap is in good accordance with prior computational calculations [19], whereas the bulk band gap value is underestimated with respect to the corresponding experimental value of 8.2 eV [26] by 23%, a discrepancy typical of approximations within DFT.

In order to explore the character of the valence and conduction band edge states, and to draw parallels between polypropelene and polyethylene, the valence and conduction band edge wavefunctions were visualized. We note that in the case of polyethylene, the valence and conduction band wavefunctions displayed interchain and intrachain character [27], consistent with its negative electron affinity [28]. However, no such clear correlations were drawn in the case of iPP, with the valence and conduction band

Table 1 The optimized geometrical parameters of iPP compared with previous DFT, and experimental works

	This work		Previous DFT work (chain) [18]	Experimental work (bulk)	
	Chain	Bulk		NMR [17]	X ray [7]
Bond length					
r_{C-C}	1.535	1.540	1.540	1.540	1.540
r_{C-H}	1.100	1.090	1.090	1.100	–
Bond angles					
CCC	109.05	111.15	–	110.00	110.00
HCH	107.56	107.64	–	109.50	–
Lattice constants					
a	–	6.39	–	–	6.65 ± 0.05
b	–	20.44	–	–	20.78 ± 0.15
c	6.49	6.47	6.49	–	6.50 ± 0.05
Unit cell angles					
β	–	99.2	–	–	99.2

All bond lengths and lattice parameters are in Å and all the angles are in degrees

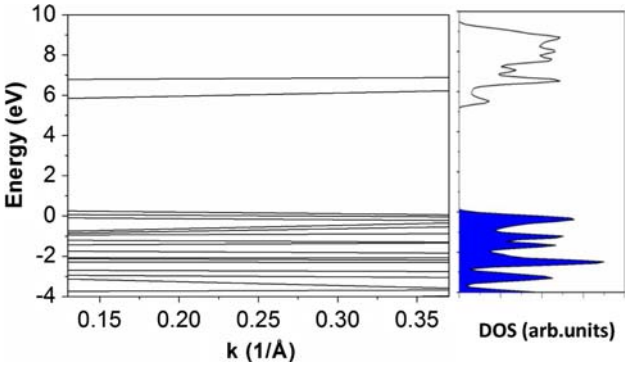

Fig. 2 Band structure and DOS of the isolated (3/1) helical iPP chain. The zero of energy is set to the valence band maximum. The shaded (unshaded) area in the DOS plot corresponds to the occupied (unoccupied) states

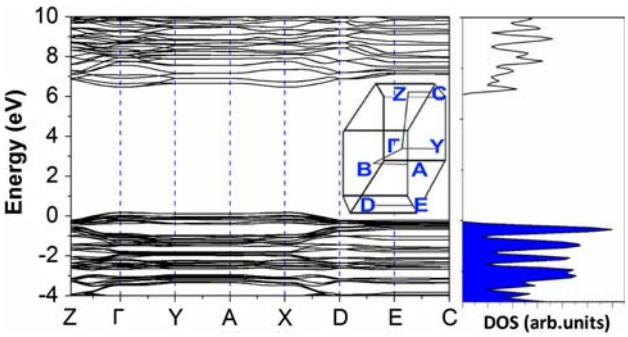

Fig. 3 Band structure and DOS of the crystalline α-iPP. The zero of energy is set to the valence band maximum. The shaded (unshaded) area in the DOS plot corresponds to the occupied (unoccupied) states

wavefunctions being more or less uniformly distributed in interchain and intrachain regions. This behavior is consistent with the electron affinity of iPP being positive (as described below).

Ionization potential and electron affinity

In analogy to the definition of the work function [29], the ionization potential IP, and the electron affinity, EA, are formally defined as

$$\mathrm{IP} = E_{\mathrm{vacuum}} - E_{\mathrm{VBM}} \quad (1)$$

$$\mathrm{EA} = E_{\mathrm{vacuum}} - E_{\mathrm{CBM}} \quad (2)$$

where E_{vacuum} is the vacuum energy level (in our case, the electrostatic potential in the vacuum region away from a surface), and E_{VBM} and E_{CBM} are, respectively, the energies of the valence band maximum (VBM) and the conduction band minimum (CBM), measured with respect to the average electrostatic potential in the bulk region sufficiently far away from the surface.

The IP and EA can be computed using standard slab supercell approaches, as has been done in the past for polyethylene [28]. Here, we specifically consider the (010) surface of α-iPP, modeled using a 40.88 Å slab (containing two unit cells along the *b*- axis, and a total of 216 atoms). The (010) surface allowed us to define a slab without the need to cleave any of the iPP chains. An alternative choice satisfying this requirement would have been the (100) surface, but this would have resulted in a slab containing almost seven times as many atoms for the same thickness as the (010) slab, and hence was not considered. With the decision on the particular surface to be considered made, two separate calculations had to be performed to determine the EA: (1) a bulk calculation that yielded the electrostatic potential (averaged along the (100) plane, so that it could be plotted along the [010] direction), and the energetic positions of the CBM and the VBM with respect to the averaged electrostatic potential, and (2) a slab calculation (with all the atomic coordinate optimized) from which the electrostatic potential, again averaged along the (010) plane.

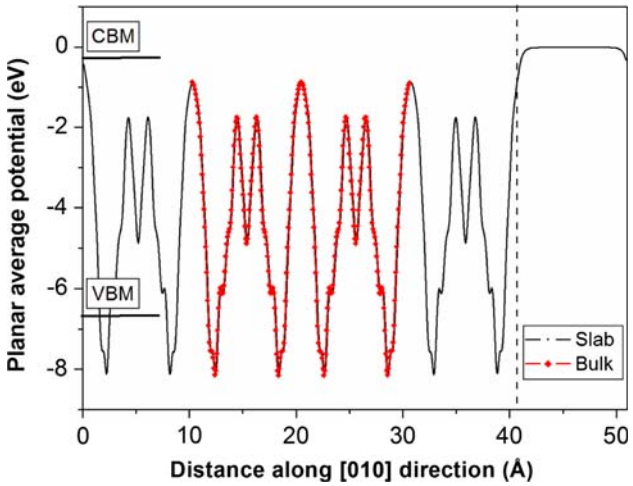

Fig. 4 Planar average potential along the [010] direction of the α-iPP bulk and a (010) slab. The zero of energy has been made to coincide with the vacuum level. The energetic positions of the CBM and VBM are fixed with respect to the bulk electrostatic potential (through a separate bulk calculation), and the CBM, VBM and the bulk electrostatic potential profile are shifted such that the bulk and slab electrostatic potentials match. The *vertical dashed line* represents the boundary between α-iPP on the left and the vacuum on the right

Figure 4 shows a plot of the planar-averaged electrostatic potential of the (010) slab. The periodic variation of the electrostatic potential within the slab, and a constant value in the vacuum region away from the slab (chosen to be the zero of energy) can be seen. Overlaid on this plot is the corresponding potential from the bulk calculation, shifted to match the slab potential profile. The perfect match between the bulk and slab results indicates that the slab is thick enough and contains a "bulk" region in its interior. The CBM and VBM are also indicated in Fig. 4 (whose positions are determined with respect to the shifted bulk electrostatic potential). From these results, IP and EA for α-iPP were determined to be 6.6 and 0.3 eV, respectively.

Chemical imperfections and electronic structure

Degradation products of polypropylene, containing carbonyl, hydroxyl and, double bond defects, have been shown to be responsible for the deterioration of the electronic properties and dielectric breakdown strength of polypropylene [30–32]. Here, we consider the impact of these impurities on the electronic structure of α-iPP. The top panel of Fig. 5 shows the location where the three types of chemical defects were successively placed. Geometry optimization was performed after placement of each defect, followed by the determination of the DOS, displayed in the bottom panel of Fig. 5. In all cases considered, a doubly occupied state and an unoccupied state were created in the band gap of α-iPP (constituting hole and electron traps, respectively). We note that in the case of the hydroxyl

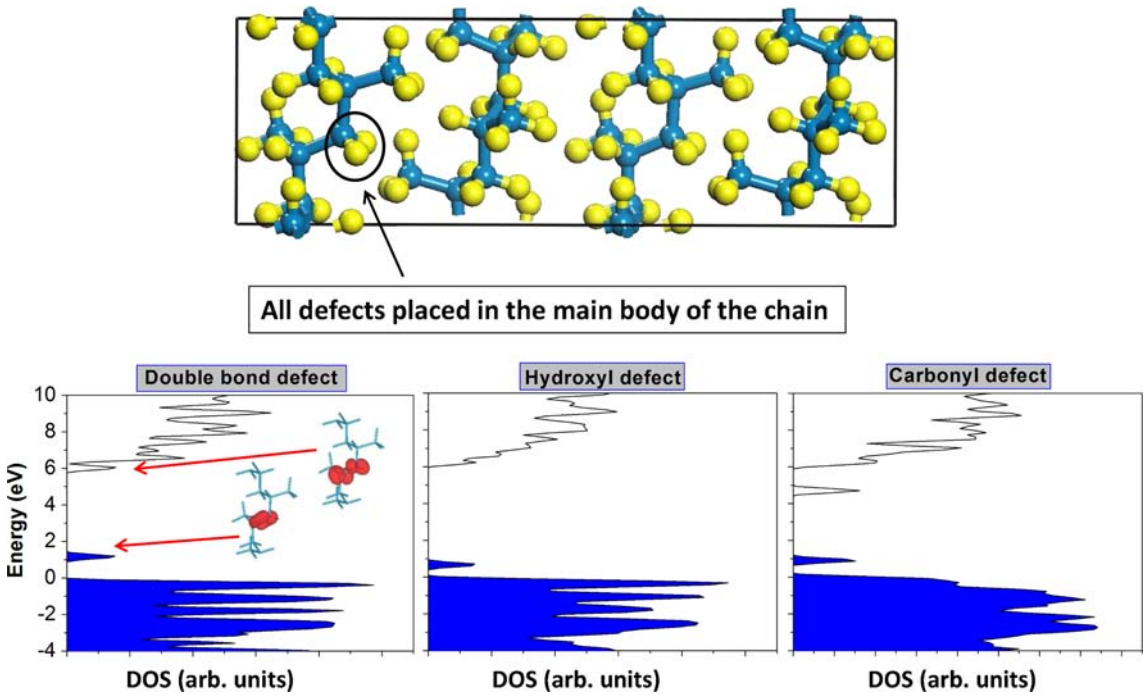

Fig. 5 *Top*: The unit cell (viewed along the *a*-axis) of α-iPP, with the location of the chemical defects (double bond, hydroxyl, or carbonyl) indicated by the circle. *Bottom*: The DOS corresponding to each impurity type. For the case of double bond impurity the occupied and unoccupied defect state orbitals are shown as insets. The shaded (unshaded) areas correspond to the occupied (unoccupied) states

defect, the unoccupied state is "mixed" with the αiPP conduction band.

In order to explore the character of the defect state orbitals, the highest occupied and lowest unoccupied state partial charge densities for the double bond defect case were visualized. These are shown as insets in the corresponding DOS plot in the bottom panel of Fig. 5. As can be seen, and as expected, the occupied defect state constitutes a σ-type interaction between the double-bonded C atoms, and the unoccupied defect state is mostly composed of a π-type interaction between the double-bonded C atoms. Similar behavior was seen for the other cases.

Of the three types of impurities considered, it is clear that the carbonyl defect results in the most well defined (and deepest) occupied and unoccupied states. These states can thus trap itinerant electrons *and* holes with ease, and are consistent with the results found earlier for polyethylene [33, 34].

Summary

We have performed DFT calculations to study the physical and electronic properties of defect-free and defective α-iPP. Our results can be summarized as follows:

- The physical structure of defect-free α-iPP is in excellent agreement with available experimental data.
- The band structure of defect-free α-iPP was computed, which yields a direct band gap of 6.3 eV, underestimated by 23% with respect to the corresponding experimental value of 8.2 eV (a discrepancy typical of approximations within DFT). The band gap of a single isolated iPP chain, although direct, was determined to be smaller than the corresponding bulk value by 0.5 eV.
- The ionization potential and electron affinity of defect-free α-iPP were calculated to be 6.6 and 0.3 eV.
- Chemical defects, such as double bond, hydroxyl, and carbonyl species in α-iPP create occupied and unoccupied states in the band gap, constituting hole and electron traps, respectively. The carbonyl defects cause the most significant impact to the band structure resulting in the deepest electron and hole trap states.

Acknowledgements The authors acknowledge financial support of this work through a grant from the Office of Naval Research, and computational support through a National Science Foundation Teragrid Resource Allocation. Useful discussions with Dr. Steve Boggs, Dr. Lei Zhu, and Dr. Janet Ho are also gratefully acknowledged.

References

1. Moore Jr EP (1996) Polypropylene handbook. Hanser/Gardner Publications, OH
2. Hirano T, Nagai I, Tanaka S, Asakura M (1998) Biaxially oriented popypropylene film and a capacitor made thereof. US patent 5724222
3. Siefried W, Janocha S, Crass G (1981) Biaxially streched popypropylene composite film and electrical insulating film made therefrom. US Patent 4283453
4. Kovalchuk AA, Shevchenko VG, Shchegolikhin AN, Nedorezova PM, Klyamkina AN, Aladyshev AM (2008) J Mater Sci 43:7132. doi:10.1007/s10853-008-3029-8
5. Kurahasi K, Matsuda Y, Miyashita Y, Demura T, Ueda A, Yoshino K (2006) Electr Engin Jpn 155:331
6. Nash JL (2004) Polym Engin Sci 28:862
7. Natta G, Corradini P (1960) Nuovo Cimen Suppl 15:59
8. Immirizi A, Iannelli P (1988) Macromolecules 21:768
9. Padden Jr FJ, Keith HD (1973) J Appl Phys 44:1217
10. Padden Jr FJ, Keith HD (1966) J Appl Phys 37:4013
11. Meille SV, Brückner S (1989) Nature 340:455
12. Ferro DR, Bruckner JS, Meille SV, Ragazzi M (1992) Macromolecules 25:5231
13. Lovinger AJ, Chua JO, Gryte CC (1977) J Polym Sci Polym Phys Ed 15:641
14. Meille SV, Ferro DR, Brilckner JS, Lovinger AJ, Paddenl FJ (1994) Macromolecules 27:2615
15. De Rosa C, Auriemma F, Corradini P (1996) Macromolecules 29:7452
16. Lacks DJ (1996) Macromolecules 29:1849
17. Rutledge GC, Suter UW (1992) Macromolecules 25:1546
18. Borrmann A, Montanari B, Jones RO (1997) J Chem Phys 106:8545
19. Ruuska H, Arola E, Kannus K, Rantala TT, Valkealahti S (2008) J Chem Phys 128:064109
20. Flamant I, Mosley DH, Deleuze M, Andre JM, Delhale J (1994) Int J Quant Chem 528:469
21. Kresse G, Furthmuller J (1996) Phys Rev B 54:11169
22. Perdew JP, Chevary JA, Vosko SH, Jackson KA, Pederson MR, Singh DJ, Fiolhais C (1992) Phys Rev B 46:6671
23. Blöchl PE (1994) Phys Rev B 50:17953
24. Kresse G, Joubert D (1999) Phys Rev B 59:1758
25. Wang YX, Arai M, Sasaki T, Fan CZ (2007) Phys Rev B 75:104110
26. Xie H, Wu X, Peng Z (1994) In: Properties and applications of dielectric materials, 4th international conference, p 39. doi: 10.1109/ICPADM.1994.413947
27. Serra S, Tossati E, Ialori S, Scandolo S, Santoro G (2000) Phys Rev B 62:4389
28. Righi MC, Scandolo S, Serra S, Iarlori S, Tosatti, Santoro G (2001) Phys Rev Lett 87:076802
29. Ramprasad R, Von Allmen P, Fonseca LC (1999) Phys Rev B 60:6023
30. Cho YS, Lee HK, Shimc MJ, Kima SW (2000) Mater Chem Phys 66:70
31. Mahrous S (2005) Polym Test 24:253
32. Allen NS (1983) Degradation and stabilization of polyolefins. Elsevier Applied Science Publishers, London
33. Meunier M, Quirke N (2001) J Chem Phys 115:2876
34. Anta LA, Mercelli G, Meunier M, Quirke N (2002) J Appl Phys 92:1002
35. Miao MS, Zhang ML, Van Doren VE, Van Alsenoy C, Martins JL (2001) J Chem Phys 115:11317